Author manuscript, published in "MICCAI Workshop on Computational Diffusion MRI (2011)"

inria-00615430, version 1 - 19 Aug 2011

Theoretical Analysis and Practical Insights on EAP Estimation via a Unified HARDI Framework

Jian Cheng[1,2], Tianzi Jiang[1], and Rachid Deriche[2]

[1] Center for Computational Medicine, LIAMA, Institute of Automation, Chinese Academy of Sciences, China
[2] Athena Project Team, INRIA Sophia Antipolis – Méditerranée, France,
jiancheng@nlpr.ia.ac.cn

Abstract. Since Diffusion Tensor Imaging (DTI) cannot describe complex non-Gaussian diffusion process, many techniques, called as single shell High Angular Resolution Diffusion Imaging (sHARDI) methods, reconstruct the Ensemble Average Propagator (EAP) or its feature Orientation Distribution Function (ODF) from diffusion weighted signals only in single shell. Q-Ball Imaging (QBI) and Diffusion Orientation Transform (DOT) are two famous sHARDI methods. However, these sHARDI methods have some intrinsic modeling errors or need some unreal assumptions. Moreover they are hard to deal with signals from different **q**-shells. Most recently several novel multiple shell HARDI (mHARDI) methods, including Diffusion Propagator Imaging (DPI), Spherical Polar Fourier Imaging (SPFI) and Simple Harmonic Oscillator based Reconstruction and Estimation (SHORE), were proposed to analytically estimate EAP or ODF from multiple shell (or arbitrarily sampled) signals. These three methods all represent diffusion signal with some basis functions in spherical coordinate and use plane wave formula to analytically solve the Fourier transform. To our knowledge, there is no theoretical analysis and practical comparison among these sHARDI and mHARDI methods. In this paper, we propose a unified computational framework, named Analytical Fourier Transform in Spherical Coordinate (AFT-SC), to perform such theoretical analysis and practical comparison among all these five state-of-the-art diffusion MRI methods. We compare these five methods in both theoretical and experimental aspects. With respect to the theoretical aspect, some criteria are proposed for evaluation and some differences together with some similarities among the methods are highlighted. Regarding the experimental aspect, all the methods are compared in synthetic, phantom and real data. The shortcomings and advantages of each method are highlighted from which SPFI appears to be among the best because it uses an orthonormal basis that completely separates the spherical and radial information.

1 Introduction

Diffusion MRI is to infer the microstructure of white matter by analyzing the diffusion weighted MRI (DWI) signals. Under the narrow pulse assumption, the Fourier trans-

This work was partially granted by the French Government Award Program, the Natural Science Foundation of China (30730035,81000634), the National Key Basic Research and Development Program of China (2007CB512305), the French ANR "Neurological and Psychiatric diseases" NucleiPark and the France-Parkinson Association.

inria-00615430, version 1 - 19 Aug 2011

form of the normalized DWI signal $E(\mathbf{q}) = \frac{S(\mathbf{q})}{S(0)}$ is the Ensemble Average Propagator (EAP) which describes the mean probability over the voxel of a displacement $\mathbf{R}$ in the effective diffusion time τ [1]. $P(\mathbf{R}) = \int E(\mathbf{q}) e^{-2\pi i \mathbf{q}\cdot\mathbf{R}} d\mathbf{q}$, where $\mathbf{q}$ is the wave vector in $\mathbf{q}$ space and $\mathbf{R}$ is the displacement vector in $\mathbf{R}$ space, $\mathbf{q} = q\mathbf{r}$, $\mathbf{R} = R\mathbf{r}$, $\mathbf{u}$ and $\mathbf{r}$ are unit vectors.

In Diffusion Tensor Imaging (DTI) [2], the EAP $P(\mathbf{R})$ under free diffusion assumption is a Gaussian distribution and the signal $E(\mathbf{q})$ could be represented by a tensor which is the covariance matrix of $P(\mathbf{R})$. Although DTI has been wildly used in clinical study, it cannot account for complex fiber configurations. Diffusion Spectrum Imaging (DSI) [3] estimates $P(\mathbf{R})$ from hundreds of samples on a dense Cartesian grid via numerical Fourier transform, which is impractical because of its long acquisition time.

Beyond DTI and DSI, Q-Ball Imaging (QBI) [4, 5] and Diffusion Orientation Transform (DOT) [6] are two famous sHARDI methods. QBI uses Funk-Radon Transform to estimate the Orientation Distribution Function (ODF) $\psi(\mathbf{u})$, from single shell data. It is model free like DSI but needs less samples. However Funk-Radon Transform brings some intrinsic modeling error, i.e. the so called blurring effect. Moreover, ODF is just one of the features of EAP and it has no radial information. DOT assumes $E(\mathbf{q})$ follows mono-exponential decay, which means single shell data contain full information for data in whole $\mathbf{q}$ space. It can analytically estimate the EAP profile $P(\mathbf{R}_0)$ for a given radius $\mathbf{R}_0$. Although the mono-exponential decay assumption has been extended into multi-exponential decay model [6], it needs many samples in radial part to estimate such a mixture of mono-exponential decay model, which makes it impractical. So far most sHARDI methods are still very hard to deal with multiple shell data. Recently, several multiple shell HARDI (mHARDI) methods, Diffusion Propagator Imaging (DPI) [7, 8], Spherical Polar Fourier Imaging (SPFI) [9–11] and Simple Harmonic Oscillator based Reconstruction and Estimation (SHORE) [12], were proposed to handle multiple shell (or even arbitrarily sampled) data. They all represent $E(\mathbf{q})$ in spherical coordinate and use plane wave formula to obtain the analytical solution for the EAP and ODF. The three mHARDI methods are closely related and seem to work better in multiple shell data than sHARDI methods. However, to our knowledge there is still no comparison among them. Moreover, mHARDI methods in [8–12] were only performed on multiple shell data. We still do not know whether they are better than those previous sHARDI methods on single shell data.

In this paper, we cast these five methods (QBI, DOT, DPI, SPFI, SHORE) in a unified framework named Analytical Fourier Transform in Spherical Coordinate (AFT-SC), and compare them in both theoretical and experimental aspects. In theoretical aspect, some criteria were proposed for evaluation. And some differences and similarities among methods were demonstrated. In experimental aspect, these methods were compared in synthetic, phantom and real data.

2 Analytical Fourier Transform in Spherical Coordinate (AFT-SC)

AFT-SC. The central idea in QBI, DOT, DPI, SPFI and SHORE is to fit the $E(\mathbf{q})$ with some function sets and find the analytical relation between signal $E(\mathbf{q})$ and EAP $P(\mathbf{R})$

Table 1. Several Kinds of Analytical Fourier Transforms in Spherical Coordinate (AFT-SC)

method	$R_k(q)$	$Q_k(\mathbf{u})$	$F_{kl}(R) = 4\pi(-i)^l \int_0^\infty R_k(q) j_l(2\pi qR) q^2 dq$	$T_{klm}(\mathbf{r})$
QBI	$R(q) = \delta(q - q_0)$	$Y_l^m(\mathbf{u})$	$F_l(R) = 4\pi(-1)^{l/2} j_l(2\pi q_0 R) q_0^2$	$Y_l^m(\mathbf{r})$
SHORE	$R_{nl}(q) = G_{nl}(q, \zeta)$	$Y_l^m(\mathbf{u})$	$F_{nl}(R) = (-1)^n G_{nl}(R, \frac{1}{4\pi^2\zeta})$	$Y_l^m(\mathbf{r})$
SPFI	$R_n(q) = G_{n0}(q, \zeta)$	$Y_l^m(\mathbf{u})$	formula (9)	$Y_l^m(\mathbf{r})$
DPI_0	$R_{0l}(q) = (\frac{q}{\sqrt{\zeta}})^l$ $R_{1l}(q) = (\frac{q}{\sqrt{\zeta}})^{-l-1}$	$Y_l^m(\mathbf{u})$	$F_{0l} = (-1)^{l/2} q_{max}^{l+1.5} \zeta^{-0.5l} R^{-1.5} J_{l+1.5}(2\pi q_{max} R)$ $F_{1l} = (-1)^{l/2} R^{-1.5} \zeta^{0.5l+0.5} (\frac{(\pi R)^{l-0.5}}{\Gamma(l+0.5)} - \frac{J_{l-0.5}(2\pi q_{max} R)}{q_{max}^{l-0.5}})$	$Y_l^m(\mathbf{r})$
DPI_1	$R_l(q) = (\frac{q^2}{\zeta})^{l/2} \exp(-\frac{q^2}{2\zeta})$	$Y_l^m(\mathbf{u})$	$F_l(R) = 2^{l+1.5} \zeta^{0.5l+1.5} \pi^{l+1.5} R^l \exp(-2\zeta\pi^2 R^2)$	$Y_l^m(\mathbf{r})$
DOT_1	$R_n(q) = (\frac{q}{\sqrt{\zeta}})^{2n}$	$Y_l^m(\mathbf{u})$	$\frac{q_{max}^{2n+l+3} \pi^{l+1.5} R^l \Gamma(1.5+0.5l+n)_1 F_2(1.5+0.5l+n; 1.5+l, 2.5+0.5l+n; -\pi^2 q_{max} R)}{(-1)^{l/2} \zeta^n \Gamma(1.5+l) \Gamma(2.5+0.5l+n)}$	$Y_l^m(\mathbf{r})$
DOT_2	$R_n(q) = (\frac{q^2}{\zeta})^n \exp(-\frac{q^2}{2\zeta})$	$Y_l^m(\mathbf{u})$	$\frac{2^{n+0.5l+1.5} \zeta^{0.5l+1.5} \pi^{l+1.5} R^l \Gamma(n+0.5l+1.5)_1 F_1(n+0.5l+1.5, l+1.5, -2\zeta\pi^2 R^2)}{(-1)^{l/2} \Gamma(l+1.5)}$	$Y_l^m(\mathbf{r})$

or ODF $\psi(\mathbf{u})$. Here we present them in the same framework, named AFT-SC. Assume $E(\mathbf{q})$ can be represented in (1) as a linear combination of functions $\{B_k(q\mathbf{u})\}$, where the basis function $B_k(q\mathbf{u}) = R_k(q)Q_k(\mathbf{u})$ separates radial part and spherical part.

$$E(\mathbf{q}) = \sum_{k=0}^{K} c_k B_k(q\mathbf{u}) = \sum_{k=1}^{K} c_k R_k(q) Q_k(\mathbf{u}) \tag{1}$$

By considering the well known plane wave formula in (2), where $j_l(x)$ is the l-th order spherical Bessel function and $Y_l^m(\mathbf{u})$ is the l order m degree Spherical Harmonics (SH), $P(\mathbf{R})$ can be represented by dual basis $\{D_k(\mathbf{R})\}$ with the same coefficients $\{c_k\}$. And $D_k(\mathbf{R})$ could be separated into radial integration $F_{kl}(R)$ and spherical integration $T_{klm}(\mathbf{r})$ in (4).

$$e^{\pm 2\pi i \mathbf{q}\cdot\mathbf{R}} = 4\pi \sum_{l=0}^{\infty} \sum_{m=-l}^{l} (\pm i)^l j_l(2\pi qR) Y_l^m(\mathbf{u}) Y_l^m(\mathbf{r}) \tag{2}$$

$$P(\mathbf{R}) = \sum_{k=0}^{K} c_k D_k(\mathbf{R}) = \sum_{k=0}^{K} \sum_{l=0}^{\infty} \sum_{m=-l}^{l} c_k F_{kl}(R) T_{klm}(\mathbf{r}) \tag{3}$$

$$F_{kl}(R) = 4\pi(-i)^l \int_0^\infty R_k(q) j_l(2\pi qR) q^2 dq \quad T_{klm}(\mathbf{r}) = \left\{ \int_{\mathbb{S}^2} Q_k(\mathbf{u}) Y_l^m(\mathbf{u}) d\mathbf{u} \right\} Y_l^m(\mathbf{r}) \tag{4}$$

Thus there is an analytical EAP estimation once $F_{kl}(R)$ and $T_{klm}(\mathbf{r})$ have closed forms. Since SH is the orthonormal basis which has been widely used in many domains such as dMRI and graphics and $E(\mathbf{q})$ and $P(\mathbf{R})$ are both antipodally symmetric, it is reasonable to choose $Q_k(\mathbf{u})$ as the real Spherical Harmonic with even l [5], which is still denoted as $Y_l^m(\mathbf{u})$ for simplicity. Then we have $T_{klm}(\mathbf{r}) = Y_l^m(\mathbf{r})$, because $\int_{\mathbb{S}^2} Y_{l'}^{m'}(\mathbf{q}) Y_l^m(\mathbf{u}) = \delta_{ll'}^{mm'}$. Then different methods can be obtained by choosing different radial functions. See table 1 for an overview and we will introduce them one by one in the following.

QBI. $E(q) = \sum_{l=0}^{L} \sum_{m=-l}^{l} c_{lm} \delta(q - q_0) Y_l^m(\mathbf{u})$ is used in QBI [4, 5, 9, 13] for a given $\mathbf{q}$ shell at $q = q_0$. The analytical form of ODF could be obtained from several ways [5, 9, 13]. In AFT-SC, $F_{kl}(R) = 4\pi(-1)^{l/2} \int_0^\infty \delta(q - q_0) j_l(2\pi qR) q^2 dq = 4\pi(-1)^{l/2} j_l(2\pi q_0 R) q_0^2$. So the EAP in QBI as well as the ODF is obtained in (5), by considering $\psi(\mathbf{r}) =$

inria-00615430, version 1 - 19 Aug 2011

$\frac{1}{Z}\int_0^\infty P(R\mathbf{r})dR$ and $\int_0^\infty j_l(x)dx = \frac{\sqrt{\pi}\Gamma(0.5l+0.5)}{2\Gamma(0.5l+1)} = (-1)^{l/2}\frac{\pi}{2}P_l(0)$, where $P_l(0)$ is the Legendre polynomial of order l at 0. The ODF formula is the same as the one in [5, 9, 13], however in AT-SC we can obtain the new form for EAP as well as ODF in QBI. To our knowledge, the EAP formula has not been proposed before in QBI.

$$P(\mathbf{R}) = \sum_{l=0}^{L}\sum_{m=-l}^{l} c_{lm}4\pi(-1)^{l/2}j_l(2\pi q_0 R)q_0^2 Y_l^m(\mathbf{r}) \quad \psi(\mathbf{r}) = \frac{q_0}{Z}\sum_{l=0}^{L}\sum_{m=-l}^{l} c_{lm}2\pi P_l(0)Y_l^m(\mathbf{r}) \tag{5}$$

SHORE. SHORE expands $E(\mathbf{q})$ into a linear combination of orthonormal basis in (6) which is the solution of 3D quantum mechanical harmonic oscillator problem [12]. Actually this basis has been already used in the computation of the molecular electron orbitals and molecular docking [14, 15, 9]. The radial part of SHORE basis with the scale ζ is shown in $G_{nl}(q,\zeta)$ (7), where $L_n^\alpha(x)$ is the generalized Laguerre polynomial [14, 15, 12]. Please note that there is a small mistake in the exponential part in [12], so we use the correct form in [14, 15]. Also please note the difference between the N in formula (6) and N_{max} in [12]. N_{max} in [12] denotes the order of polynomial in radial part which is $2N$ in our notation. Interestingly, the radial integration is analytically obtained as the same form by using the property of Laguerre polynomial [16].

$$E(\mathbf{q}) = \sum_{n=0}^{N}\sum_{l=0}^{n}\sum_{m=-l}^{l} c_{nlm}G_{nl}(q,\zeta)Y_l^m(\mathbf{u}) \quad P(\mathbf{R}) = \sum_{n=0}^{N}\sum_{l=0}^{n}\sum_{m=-l}^{l} c_{nlm}(-1)^n G(R,\frac{1}{4\pi^2\zeta})Y_l^m(\mathbf{r}) \tag{6}$$

$$G_{nl}(q,\zeta) = \kappa_{nl}(\zeta)(\frac{q^2}{\zeta})^{l/2}\exp\left(-\frac{q^2}{2\zeta}\right)L_{n-l/2}^{l+1/2}(\frac{q^2}{\zeta}) \qquad \kappa_{nl}(\zeta) = \left[\frac{2}{\zeta^{3/2}}\frac{(n-l/2)!}{\Gamma(n+l/2+3/2)}\right]^{1/2} \tag{7}$$

SPFI. SPFI was first proposed in [9] with a numerical EAP estimation. Then the analytical solution was given in [11]. The signal in SPFI is represented in (8) which is closely related with SHORE. However, the radial integration $F_{nl}(R)$ shown in (9) is totally different from SHORE, where ${}_1F_1$ is the confluent hypergeometric function [11].

$$E(\mathbf{q}) = \sum_{n=0}^{N}\sum_{l=0}^{L}\sum_{m=-l}^{l} c_{nlm}G_{n0}(q,\zeta)Y_l^m(\mathbf{u}) \qquad P(\mathbf{R}) = \sum_{n=0}^{N}\sum_{l=0}^{L}\sum_{m=-l}^{l} c_{nlm}F_{nl}(R)Y_l^m(\mathbf{r}) \tag{8}$$

$$F_{nl}(R) = \frac{\zeta^{0.5l+1.5}\pi^{l+1.5}R^l\kappa_{n0}(\zeta)}{(-1)^{l/2}\Gamma(l+1.5)}\sum_{i=0}^{n}\binom{n+0.5}{n-i}\frac{(-1)^i}{i!}2^{0.5l+i+1.5}\Gamma(0.5l+i+1.5)\,{}_1F_1(\frac{2i+l+3}{2};l+\frac{3}{2};-2\pi^2R^2\zeta) \tag{9}$$

DPI$_0$. DPI in [8], called DPI$_0$ here, assumes the signal $E(\mathbf{q})$ is the solution of 3D Laplace equation, i.e. $E(\mathbf{q}) = \sum_{n=0}^{1}\sum_{l=0}^{L}\sum_{m=-l}^{l} c_{nlm}R_{nl}(q)Y_l^m(\mathbf{u})$, where $R_{0l}(q) = (\frac{q}{\sqrt{\zeta}})^l$ and $R_{1l}(q) = (\frac{q}{\sqrt{\zeta}})^{-l-1}$. Please note that here we introduce the scale parameter ζ in DPI$_0$ motivated by SHORE and SPFI. It is the same as the original DPI in [7, 8] if $\zeta = 1$. If $\zeta \neq 1$, it is equivalent with the original one but more numerically stable when an appropriate ζ is chosen. For the original DPI, one need to choose carefully the unit for numerical stability in least square estimation as suggested by the authors [8]. Here we can choose a scale ζ so that $q/\sqrt{\zeta}$ is independent with unit. Experimentally we choose

inria-00615430, version 1 - 19 Aug 2011

$\zeta = 0.5q_{max}^2$ for good numerical stability, where q_{max} is the maximum q value for DWI signals. In DPI_0, the radial integration $F_{nl}(R)$ can not be analytically solved, and the author in [8] introduced q_{max} and approximate $F_{nl}(R)$ using the integration from 0 to q_{max}, which could be found in table 1 [8]. Beyond DPI_0, we propose DPI_1 which only uses regular terms in DPI_0, i,e, $E(\mathbf{q}) = \sum_{l=0}^{L}\sum_{m=-l}^{l} c_{lm}R_l(q)Y_l^m(\mathbf{u})$, $R_l(q) = (\frac{q}{\sqrt{\zeta}})^l$. We will discuss it later.

DOT_0 and DOT_1. The original DOT, called DOT_0 here, assumes $E(\mathbf{q})$ follows mono-exponential decay [6], i.e. $E(\mathbf{q}) = \exp(-4\pi^2q^2A(\mathbf{u}))$. Actually DOT_0 cannot be contained in AFT-SC framework because $E(\mathbf{q})$ in DOT cannot be separated into radial part and spherical part (1). The author in [6] analytically solved the radial integration in (10) for the given samples $\{E(\mathbf{q}_i)\}$. Then the inner product between $I_l(R,\mathbf{u})$ and $Y_l^m(\mathbf{u})$ in the spherical integration (11) was solved numerically using least square fitting for the samples $\{I_l(R,\mathbf{u}_i)\}$ obtained in (10).

$$I_l(R,\mathbf{u}) = 4\pi(-1)^{l/2}\int_0^\infty E(\mathbf{q})j_l(2\pi qR)q^2dq = \frac{R^l\Gamma(0.5l+1.5)_1F_1(0.5l+1.5,l+1.5,-\frac{R^2}{4\tau A(\mathbf{u})})}{(-1)^{l/2}2^{l+1}\pi^{0.5}(A(\mathbf{u})\tau)^{0.5l+1.5}\Gamma(l+1.5)} \tag{10}$$

$$P(\mathbf{R}) = \left\{\int_{\mathbb{S}^2} I_l(R,\mathbf{u})Y_l^m(\mathbf{u})d\mathbf{u}\right\}Y_l^m(\mathbf{r}) \tag{11}$$

Please note there is no full representation for $E(\mathbf{q})$ and $P(\mathbf{R})$, because one needs to re-estimate $P(\mathbf{R})$ in different R. Although DOT_0 is not contained in AFT-SC, it is still possible to explain DOT_0 in AFT-SC framework. We can represent $A(\mathbf{u}) = \sum_{lm} a_l^m Y_l^m(\mathbf{u})$ and expand $E(\mathbf{q}) = \sum_{n=1}^{\infty}\frac{(-4\pi^2q^2)^n}{n!}(\sum_{lm} a_l^m Y_l^m(\mathbf{u}))^n = \sum_{nlm} c_{nlm}q^{2n}Y_l^m(\mathbf{u})$, where c_{nlm} can be analytically obtained from a_l^m by expanding the product of two SHs in terms of SHs itself with the Clebsch-Gordan coefficients. We call the modified representation of DOT as DOT_1, which separates spherical part and radial part. DOT_1 is equivalent with DOT_0 if $\{a_l^m\}$ is estimated from DWI samples and $\{c_{nlm}\}$ is calculated from $\{a_l^m\}$. But alternatively we can fit the signal directly with the representation $E(\mathbf{q}) = \sum_{nlm} c_{nlm}(\frac{q^2}{\zeta})^n Y_l^m(\mathbf{u})$, where ζ is the fixed scale parameter. In this case DOT_1 is not DOT any more and more similar with DPI. It does not assume mono-exponential decay and works for multiple shell data. Similarly with DPI there is no analytical form for radial integration. Thus we introduce q_{max} for the integration from 0 to q_{max} [16]. See table 1, where ${}_1F_2$ is the generalized hypergeometric function.

3 Theoretical Comparisons

Based on AFT-SC framework, it seems to be an easy job to deduce an analytical EAP reconstruction and we can have many analytical EAP estimation including the given five. Then which one is better? We propose some criteria for evaluation.

Completeness. In AFT-SC, $E(\mathbf{q})$ is represented by a linear combination of some basis functions $\{B_i(\mathbf{q})\}$ in (1). $\{B_i(\mathbf{q})\}$ is complete if it can represent any symmetric square integrable $E(\mathbf{q})$ in 3D space. Completeness means more samples we have, better reconstruction we get. If all DWI samples are known in whole $\mathbf{q}$ space, the samples will be fitted without any modeling error. QBI assumes $E(\mathbf{q})$ exists only on the sphere

inria-00615430, version 1 - 19 Aug 2011

$\mathbb{S}^2$ and DOT_0 assumes mono-exponential decay, so QBI and DOT_0 are not complete in $\mathbb{R}^3$. SHORE basis is complete because it is the eigenfunction of Sturm-Liouville equation. SPF basis is complete because $\{Y_l^m(\mathbf{u})\}$ is complete in $\mathbb{S}^2$ and $L_n^{1/2}(x)$ is complete in $[0,\infty)$ with the weight $x^{1/2}\exp(-x)$. DPI_0 is not complete because not every function satisfies Laplace's equation. Based on Weierstrass theorem the continuous $E(\mathbf{q})$ in the ball with a given radius can be uniformly approximated by a polynomial function, i.e. $E(\mathbf{q}) = \sum_{ijk} a_{ijk} q_x^i q_y^j q_z^k$. Because $E(\mathbf{q})$ is symmetric, $i+j+k$ is even, say $2n$. Then by representing every monomial via spherical coordinate, we have $E(\mathbf{q}) = \sum_{nlm} c_{nlm}(\frac{q}{\sqrt{\zeta}})^{2n} Y_l^m(\mathbf{u})$, which means the basis in DOT_1 is complete for $E(\mathbf{q})$ inside a ball. However for both DPI and DOT_1, since only finite terms are used, the represented $E(\mathbf{q})$ tends to ∞ as q increases. It contradicts with the fact that $E(\mathbf{q})$ tends to 0 when q increases, which means DPI and DOT_1 have intrinsic modeling error in the region with large q. So the q_{max} is needed for an incomplete integration. However, if q_{max} is chosen as the maximal q values of DWI signals like [8], the estimated EAPs are less anisotropic because of incomplete integration, which means DPI_0 and DOT_1 cannot work well with DWIs with only small b values. And if q_{max} is chosen as a large value, the estimated EAPs are likely noisy because of the modeling error in the area with large q value.

Representability. We know three priors (P1, P2 and P3) for $E(\mathbf{q})$. **P1**: $E(0) = 1$ because $\int_{\mathbb{R}^3} P(\mathbf{R}) d\mathbf{R} = 1$. **P2**: $E(\mathbf{q})$ tends to 0 when q tends to ∞. **P3**: $E(\mathbf{q})$ radially decays like (but NOT) a Gaussian. Please note that the estimated $P(\mathbf{R})$ is *globally* affected by $E(\mathbf{q})$ in whole $\mathbf{q}$ space because Fourier Transform is a global transform. So even though one method can fit the given samples of the DWI well, it does not mean the estimated EAP is good. For the signal fitting in existing works, the given samples have been well considered. The results will be better if the model can also consider these priors. The model which satisfies these priors has good results, even if it is not complete, e.g. mixture of tensor model. QBI satisfies none of the priors. In practice we find the EAP in QBI has many negative values especially when $R > 10\mu m$, which is probably because QBI is lack of representability. DOT_0 automatically considers the first two, while it assumes mono-exponential decay. SHORE and SPFI consider the second and third in their model. For $E(0) = 1$, SHORE, SPFI and DOT_1 can add the shell of $b = 0$ into estimation process as suggested in [11, 10]. While DPI cannot consider $b = 0$ in estimation because $E(0)$ does not exist in DPI model. Moreover, in DPI as well as DOT_1 $E(\mathbf{q})$ tends to ∞ when q increases and many radial terms are needed if one uses polynomials to approximate a Gauss-like decay. So even though DPI may fit the given DWI signals well as shown in [8], the estimated EAP is problematic. Motivated by SHORE and SPFI, we can avoid the problem by adding exponential term into DPI and DOT_1 and ignoring irregular terms in DPI. Then we have two new methods, DPI_1 where $E(\mathbf{q}) = \sum_{lm} c_{lm}(\frac{q^2}{\zeta})^{l/2}\exp(-\frac{q^2}{2\zeta})Y_l^m(\mathbf{u})$, and DOT_2 where $E(\mathbf{q}) = \sum_{nlm} c_{nlm}(\frac{q^2}{\zeta})^n \exp(-\frac{q^2}{2\zeta})Y_l^m(\mathbf{u})$. Similarly with SHORE and SPFI, they both satisfy all three priors. And DOT_2 is equivalent with SPFI because after Gram-Schmidt orthonormalization in radial part, DOT_2 will become SPFI. So DOT_2 is complete. While DPI_1 is not because DPI_1 now assumes $E(\mathbf{q})$ is a harmonic polynomial multiplied by a Gaussian. DOT_2 and DPI_1 both have analytical EAP forms based on the result in [11] and we do not need q_{max} any more. See table 1.

inria-00615430, version 1 - 19 Aug 2011

inria-00615430, version 1 - 19 Aug 2011

Separation information between spherical and radial parts. Please note the important difference between the basis functions in SHORE, SPFI and DPI_0. DPI_0 is lack of representability partially because it coupled radial information and spherical information together. For example DPI_0 cannot represent an isotropic Gaussian function, because isotropic function forces $l = 0$ in SHs in spherical part, then in radial part $R_{00} = 1$ and $R_{10} = (\frac{q}{\sqrt{\zeta}})^{-1}$ which contradict with Gaussian function. In SPFI the radial part and spherical part are completely separated, which allows one chooses higher order in spherical part but low order in radial part. While in SHORE, $n - l/2 \geq 0$ is forced in (6), which means for a given l in spherical part, the corresponding order of power in radial part is $2n \geq l$. In SPFI, the minimal order for anisotropy diffusion is $N = 1$, $L = 4$, which means it contains SH of order $0, 2, 4$ and power $0, 2$ in radial part. In SHORE, the minimal order is $N = 2$ ($N_{max} = 4$ in [12]), which means it contains SH of order $0, 2, 4$ and power $0, 2, 4$ in radial part. Besides it can be proved that the functional space spanned by SHORE basis $\{G_{nl}Y_l^m\}_{n\leq N}$ with order $n \leq N$ is a subspace of the space spanned by SPF basis $\{G_{n0}Y_l^m\}_{n\leq N, l\leq 2N}$ with radial order $n \leq N$ and spherical order $l \leq 2N$. Thus if order N is enough to represent the signal in SHORE, radial order N and spherical order $2N$ is also enough for representation in SPF basis. However if limited samples with low SNR are given for estimating the coefficients, a truncated basis is needed to avoid overfitting. Then SHORE basis with higher power order in radial part may have some overfitting effects, and the effect will be enhanced when larger N (6 or 8) is used.

Orthogonality and stability. In approximation theory, complete orthonormal basis is preferred because monomial basis is known to have poor numerical stability and the coefficients under orthonormal basis are independent with the basis order chosen in Least Square approximation if all samples are known. For example, if exhaustive samples of diffusion signal are known in a single shell, the coefficients under Spherical Harmonics are independent with the chosen order in least square fitting, while the coefficients under High Order Tensor basis is dependent on the chosen order [17], although these two bases are both complete in $\mathbb{S}^2$. The bases in DOT_1 DOT_2 and DPI_0 DPI_0 are not orthogonal. SHORE and SPFI use orthonormal bases in $\mathbb{R}^3$ while QBI and DOT_0 uses orthonormal bases only in $\mathbb{S}^2$. When orthonormal basis $\{B_k(\mathbf{q})\}$ is used to represent $E(\mathbf{q})$, its Fourier dual basis $\{D_k(\mathbf{R})\}$ that represents $P(\mathbf{R})$ is still orthonormal because of the Parseval's theorem.

Single shell and multiple shells. These mHARDI methods can work for multiple shell data. However, when only single shell data are given, these methods are unstable. Let's take SPFI as an example. In SPFI, for a given q_0, the ratio between two basis functions $\frac{R_n(q_0)Y_l^m(\mathbf{u})}{R_{n'}(q_0)Y_l^m(\mathbf{u})}$ is a constant independent with $\mathbf{u}$, which means these two basis functions with same l and m but different n are undistinguishable for single shell data. When least square is used to estimate the coefficients, the basis matrix is rank deficient with very large conditional number. To solve this problem, one can consider the shell of $b = 0$, which means two shells are used for single shell data [11, 10]. However, DPI_0 can not consider $b = 0$, so it is unstable.

Summary. SHORE and SPFI use 3D complete orthonormal basis and have the best representability. SHORE require higher orders in radial part than SPFI which completely separate the information between spherical and radial part. SHORE and SPFI

Table 2. Some Criteria for Evaluating Methods. P1, P2 and P3 are three priors.

method	$R_k(q)$	$Q_k(\mathbf{u})$	Completeness	P1	P2	P3	orthogonal	single shell	Separation
QBI	$R(q) = \delta(q - q_0)$	$Y_l^m(\mathbf{u})$	in $\mathbb{S}^2$	No	No	No	in $\mathbb{S}^2$	Yes	Yes
SHORE	$R_{nl}(q) = G_{nl}(q, \zeta)$	$Y_l^m(\mathbf{u})$	Yes	Yes	Yes	Yes	Yes	Yes	No
SPFI	$R_n(q) = G_{n0}(q, \zeta)$	$Y_l^m(\mathbf{u})$	Yes	Yes	Yes	Yes	Yes	Yes	Yes
DPI_0	$R_{0l}(q) = (\frac{q}{\sqrt{\zeta}})^l$ $R_{1l}(q) = (\frac{q}{\sqrt{\zeta}})^{-l-1}$	$Y_l^m(\mathbf{u})$	No	No	No	No	No	No	No
DPI_1	$R_l(q) = (\frac{q^2}{\zeta})^{l/2} \exp(-\frac{q^2}{2\zeta})$	$Y_l^m(\mathbf{u})$	No	Yes	Yes	Yes	No	Yes	No
DOT_1	$R_n(q) = (\frac{q^2}{\zeta})^n$	$Y_l^m(\mathbf{u})$	in a ball	Yes	No	No	No	Yes	Yes
DOT_2	$R_n(q) = (\frac{q^2}{\zeta})^n \exp(-\frac{q^2}{2\zeta})$	$Y_l^m(\mathbf{u})$	Yes	Yes	Yes	Yes	No	Yes	Yes
DOT_0	—	—	in $\mathbb{S}^2$	Yes	Yes	No	in $\mathbb{S}^2$	Yes	Yes

are well appropriate for both single and multiple shell data, while DPI_0 is unstable in single shell data and work only for multiple shell data with large b values. Please see Table 2 for more information.

4 Experimental Comparisons

Due to limited space, we only compare QBI, DOT_0, DPI_0, SPFI and SHORE in experiments. Please note that SHORE uses quadratic programming with nonnegative constraints to estimate the coefficients [12]. Actually all these five methods can use convex optimization with constraints for a better reconstruction. However, to perform a fair comparison, we implement SHORE and SPFI via least square with regularization λ_l in spherical part and λ_n in radial part and the scale ζ is set from typical diffusion coefficient as suggested in SPFI [9, 11, 10]. Least square with Laplace-Beltrami regularization is used for QBI, DOT_0 and DPI_0 [5, 6, 8]

Synthetic data. We generate synthetic data using Söderman cylinder model [6]. The parameters are set as the same in [6]: length $L = 5mm$, radius $\rho = 5\mu m$, free diffusion coefficient $D_0 = 2.02 \times 10^{-3} mm^2/s$, $\Delta/\delta = 20.8/2.4ms$. DWI data were generated in 3 shells with b value $500/1500/3000 s/mm^2$, 60 evenly distributed samples per shell.

In the noise free experiment, the data was generated from two fibers crossing with 90^o along x-axis and y-axis. The ground truth signal in x-y plane was visualized in Fig. 1, which also showed the reconstructed signals in the five methods. $L = 8$ and $\lambda_l = 10^{-9}$ were set for QBI, DOT_0 and DPI_0, $L = 8$, $N = 4$ and $\lambda_l = \lambda_n = 10^{-9}$ for SPFI and SHORE. For DOT_0, the signal samples on single shell of $b = 1500 s/mm^2$ suggested in [6] was used to extrapolate the signal in other positions based on mono-exponential decay assumption. The single shell samples was also used to estimate the coefficients for QBI. Please note in QBI, the signal inside and outside the q-ball was forced to zero as we have discussed. Three shell samples were used in DPI_0, SPFI and SHORE. We also plotted the values along given two lines where Line1 is along y-axis and Line2 has 45^o azimuth. In Line1, the curves obtained from SPFI and SHORE are more closed to the ground truth and better than DOT_0. while in Line2 SPFI, SHORE and DOT_0 obtained very similar results with the ground truth. DPI_0 gave the worst results where signal tends to infinity as q increases, the origin point is singular, and the signal near the

inria-00615430, version 1 - 19 Aug 2011

inria-00615430, version 1 - 19 Aug 2011

Fig. 1. The left side shows the ground truth signal and the reconstructed signals from 5 methods in x-y plane. Please note the origin point in DPI is singular, so we set it as the mean of the 4 points in its neighborhood. The right side shows the signal values on two lines (Line1 and Line2).

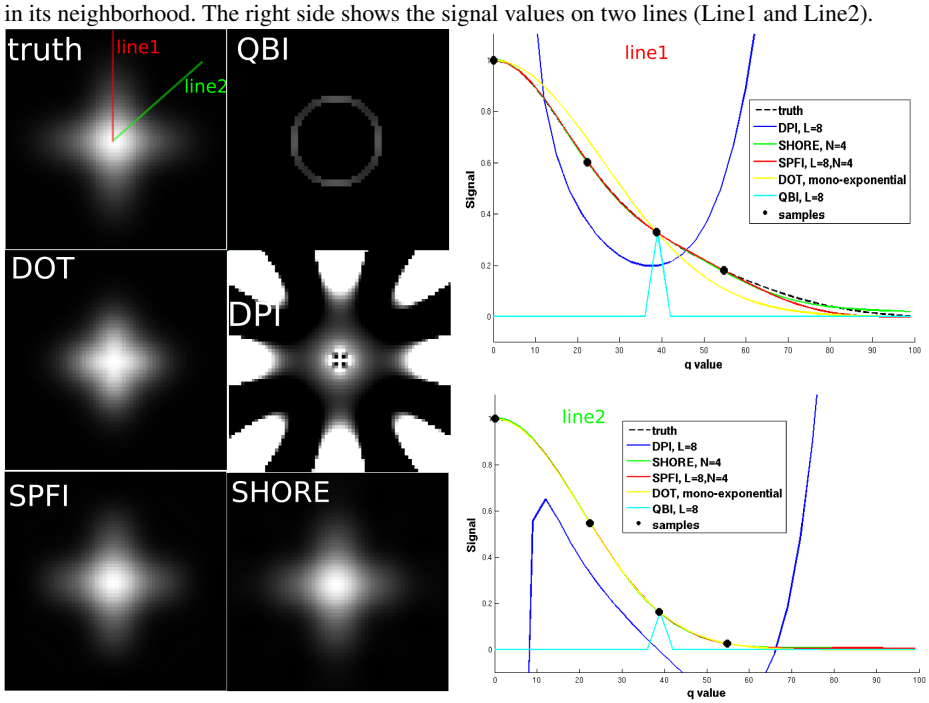

origin has unacceptable very large absolute value. The reconstructed signal from DPT_0 is a polynomial along each direction, not a Gaussian-like decay. QBI only considers the signal in the q-ball and does not extrapolate signal in q-space, which is inappropriate for EAP estimation since Fourier transform is a global transform.

The performance on detecting fiber directions of the five methods were compared with the data corrupted by Rician noise. The noise was added for 1000 trials with SNR=10. EAP profile at $15\mu m$ was estimated from DOT_0, DPI_0, SPFI and SHORE. ODF instead of EAP in QBI was estimated because EAP in QBI has many negative values especially when $R > 10\mu m$. The maxima of EAP profiles or ODFs were detected. And the successful ratio to detect 2 maxima was recorded. The mean difference of angle (MDA) was calculated from the successful trials. An truncated basis is needed for the data corrupted by noise. For DOT_0, QBI and DPI_0 we set $L = 4$ and $\lambda_l = 0.006$ suggested in [5]. For SPFI, $L = 4$, $N = 1$ and $\lambda_l = \lambda_n = 1e-8$ suggested in [11]. For SHORE, please note that $N = 3$ ($N_{max} = 6$ in [12]) used in [12] does not work well when SNR= 10. Thus we set $N = 2$ ($N_{max} = 4$) and $\lambda_l = \lambda_n = 1e-8$ for SHORE similarly with SPFI. Fig. 2 shows the results of SPFI, SHORE and DPI using 3 shells and the results of five methods using only single shell at $b = 1500 s/mm^2$. We use the shell at $b = 1500 s/mm^2$ because the data at $3000 s/mm^2$ has relatively lower SNR and

Fig. 2. A: success ratio (solid lines) and MDA (dashed lines) for SPFI, SHORE and DPI in 3 shells; B: success ratio for five methods in single shell with $b = 1500$; C: MDA for five methods in single shell with $b = 1500$.

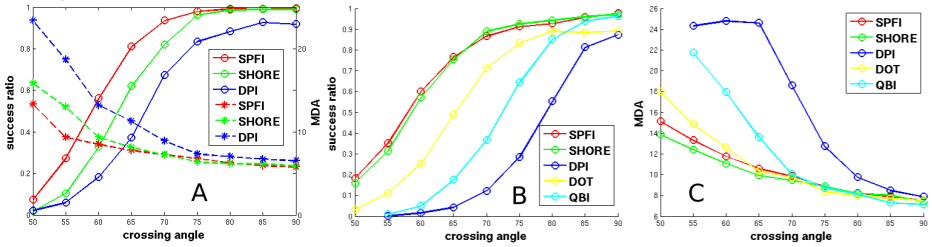

1500 was suggested for DOT in [6]. It is clear in Fig. 2 that SPFI has best results among mHARDI methods using 3 shell data, while it has similar results with SHORE in single shell data. SPFI and SHORE obtain better results even for single shell data than other methods. DOT and QBI are better than DPI in single shell data, probably because DPI is unstable in single shell data, or because q_{max} calculated from $b = 1500$ is small considering the maximal b value 8000 is used in [8]. It is worth to see that for SHORE and SPFI when crossing angle is small the results from single shell data are a little better than the results from three shells. It is probably because the data at $b = 3000$ have too much noise and relatively low SNR.

Phantom data. The five methods were performed on the *public* phantom data with 3 shells ($500/1500/2000 s/mm^2$) which was used in Fiber Cup in MICCAI 2009 [18]. The same parameters were used in methods as the above synthetic data. EAPs at $15\mu m$ were estimated from 3 shells in SPFI, SHORE and DPI and from single shell with $b = 2000 s/mm^2$ in DOT. The single shell data was also used to estimate ODF in QBI. The ground truth of fiber directions was shown in Fig. 3. And two regions (R1, R2) were enlarged to show the EAP profiles ODFs. Compare to the ground truth, SPFI and SHORE work well in two regions and they have similar results. The results of DPI are much smooth. DOT and QBI has smooth results in R1 but noisy results in R2.

Real data. The five methods were also compared on a real monkey data with 3 shells ($500/1500/3000\ s/mm^2$). Each shell has only 30 samples. The same parameters were used in methods as the synthetic and phantom data. EAPs at $15\mu m$ were estimated from 3 shells in SPFI, SHORE and DPI and from single shell with $b = 1500$ in DOT. ODFs in QBI were estimated from the signal shell data. An enlarged region was shown in Fig. 3. GFA map [4] is calculated in each method and used for the glyph color and background. Please note that we did not perform min-max normalization [4, 5], so ODFs in QBI are less anisotropic. EAPs in DPI are also less anisotropic, because we did not do normalization like [8] and the maximal b value for q_{max} used here is 3000, while 8000 is used in [8]. SHORE and SPFI have similar results which are better than DOT and others. The result from SHORE seems to have sharper glyphs than SPFI. To test our discussions on the difference between SHORE and SPFI, we add Rician noise with SNR=20 to the original DWI data, then estimate the EAPs from the noisy data. For the noisy data, SHORE obtains noisy results especially in isotropic regions, which vali-

inria-00615430, version 1 - 19 Aug 2011

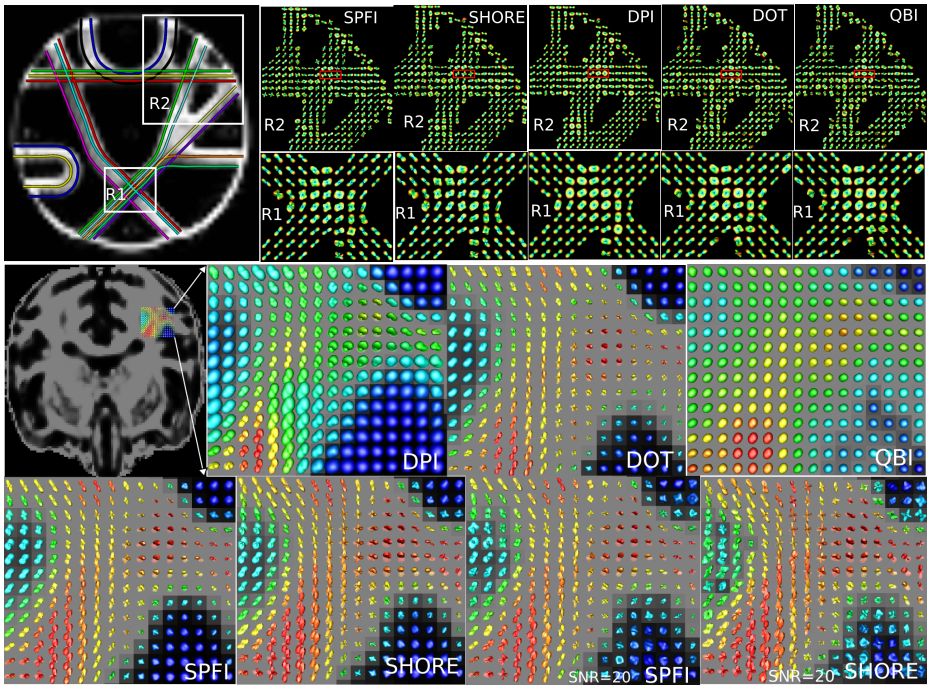

Fig. 3. The first row is for phantom data. From left to right: the ground truth of fiber direction, and the EAPs/ODFs in two enlarged regions R1 and R2 under 5 methods. A crossing area is highlighted in red box. The second and third rows are for real data. From left to right: GFA map calculated from EAP in SPFI and an enlarged region with EAPs/ODFs in five methods. The results from original data and noisy data using SPFI and SHORE were shown in the third row. GFA map is calculated from the glyphs and used for the glyph color and background.

dates our previous discussion that SHORE probably has some overfitting effect because it forces higher order in radial part than SPFI. This effect may result in more crossings which are false positive. The result from noisy data in SPFI is very similar with the result from the original data, which means SPFI is robust to noise because low order is used in radial part.

5 Conclusion

In this paper, we proposed a unified computational framework named Analytical Fourier Transform in Spherical Coordinate (AFT-SC) to analyse and compare state-of-the-art single and multi-shell Ensemble Average Propagator estimation methods in High Angular Resolution Diffusion Imaging. Three mHARDI methods (DPI, SPFI, SHORE) and two sHARDI methods (QBI, DOT) were compared both theoretically and experimentally on synthetic, phantom and real data. With respect to the theoretical aspect, some criteria have been proposed for evaluation, including completeness, representability, separation information between spherical and radial parts, orthogonality and stability.

inria-00615430, version 1 - 19 Aug 2011

Some differences and similarities among the methods have been highlighted. For instance, we have shown that DPI is unstable in single shell data while SHORE requires high order in radial part. The experiments have shown that SHORE and SPFI are the best for single shell data, while DPI only works for multiple shell data with large b values. For multi-shell, SPFI appears to perform better than SHORE and the other methods, partly due to the fact that it uses an appropriate orthonormal basis that completely separates the spherical and radial information.

References

1. Callaghan, P.T.: Principles of nuclear magnetic resonance microscopy. Oxford University Press (1991)
2. Basser, P.J., Mattiello, J., LeBihan, D.: MR diffusion tensor spectroscropy and imaging. Biophysical Journal **66** (1994) 259–267
3. Wedeen, V.J., Hagmann, P., Tseng, W.Y.I., Reese, T.G., Weisskoff, R.M.: Mapping Complex Tissue Architecture With Diffusion Spectrum Magnetic Resonance Imaging. Magnetic Resonance In Medicine **54** (2005) 1377–1386
4. Tuch, D.S.: Q-ball imaging. Magnetic Resonance in Medicine **52** (2004) 1358–1372
5. Descoteaux, M., Angelino, E., Fitzgibbons, S., Deriche, R.: Regularized, Fast and Robust Analytical Q-ball Imaging. Magnetic Resonance in Medicine **58** (2007) 497–510
6. Özarslan, E., Shepherd, T.M., Vemuri, B.C., Blackband, S.J., Mareci, T.H.: Resolution of complex tissue microarchitecture using the diffusion orientation transform (DOT). NeuroImage **31** (2006) 1086–1103
7. Descoteaux, M., Deriche, R., Bihan, D.L., Mangin, J.F., Poupon, C.: Diffusion Propagator Imaging: Using Laplace's Equation and Multiple Shell Acquisitions to Reconstruct the Diffusion Propagator. In: IPMI. (2009)
8. Descoteaux, M., Deriche, R., Bihan, D., Mangin, J., Poupon, C.: Multiple q-Shell Diffusion Propagator Imaging. Medical Image Analysis (2010)
9. Assemlal, H.E., Tschumperlé, D., Brun, L.: Efficient and robust computation of PDF features from diffusion MR signal. Medical Image Analysis **13** (2009) 715–729
10. Cheng, J., Ghosh, A., Deriche, R., Jiang, T.: Model-Free, Regularized, Fast, and Robust Analytical Orientation Distribution Function Estimation. In: MICCAI (2010)
11. Cheng, J., Ghosh, A., Jiang, T., Deriche, R.: Model-free and Analytical EAP Reconstruction via Spherical Polar Fourier Diffusion MRI. In: MICCAI (2010)
12. Ozarslan, E., Koay, C., Shepherd, T., Blackband, S., Basser, P.: Simple harmonic oscillator based reconstruction and estimation for three-dimensional q-space mri. In: ISMRM (2009)
13. Hess, C.P., Mukherjee, P., Han, E.T., Xu, D., Vigneron, D.B.: Q-Ball Reconstruction of Multimodal Fiber Orientations Using The Spherical Harmonic Basis. Magnetic Resonance In Medicine **56** (2006) 104–117
14. Ritchie, D., Kemp, G.: Protein docking using spherical polar Fourier correlations. Proteins: Structure, Function, and Bioinformatics **39**(2) (2000) 178–194
15. Huzinaga, S.: Gaussian-Type Functions for Polyatomic Systems. I. The Journal of Chemical Physics **42** (1965) 1293
16. Gradshteyn, I., Ryzhik, I.: Table of Integrals, Series, and Products. Elsevier (2007)
17. Özarslan, E., Mareci, T.: Generalized diffusion tensor imaging and analytical relationships between diffusion tensor imaging and high angular resolution diffusion imaging. Magnetic Resonance in Medicine (5) 955–965
18. Poupon, C., Rieul, B., Kezele, I., Perrin, M., Poupon, F., Mangin, J.: New diffusion phantoms dedicated to the study and validation of high-angular-resolution diffusion imaging (HARDI) models. Magnetic Resonance In Medicine **60(6)** (2008) 1276–1283

inria-00615430, version 1 - 19 Aug 2011